AJNR

Microanatomy of the excised human spinal cord and the cervicomedullary junction examined with high-resolution MR imaging at 9.4 Tesla.

E Beuls, J Gelan, M Vandersteen, P Adriaensens, L Vanormelingen and Y Palmers

AJNR Am J Neuroradiol 1993, 14 (3) 699-707
http://www.ajnr.org/content/14/3/699

Microanatomy of the Excised Human Spinal Cord and the Cervicomedullary Junction Examined with High-Resolution MR Imaging at 9.4 Tesla

E. Beuls,[1,3,5] J. Gelan,[2] M. Vandersteen,[1] P. Adriaensens,[2] L. Vanormelingen,[1] and Y. Palmers[1,4]

PURPOSE: To study in detail the MR anatomy of the spinal cord and the cervicomedullary junction that could serve as a reference for clinical MR studies. **METHODS:** Specimens of fresh human spinal cord and formalin-fixed cervicomedullary transition zones were imaged with a 9.4-T vertical bore magnet. Using a multisection spin-warp pulse sequence the parameters were selected to produce essentially proton density images. **RESULTS:** The images obtained depict the microanatomical organization of the spinal cord and cervicomedullary junction. In the spinal cord, the central gray has the expected higher signal intensity compared with the white matter, which is, apart from its darker general appearance, characterized by the presence of a dense radially structured neuroglial framework of high signal intensity. Anatomically more complex regions such as the dorsal root entry zone, the adjacent posterior horn complex, and the crossing fibers of the cervicomedullary junction are seen as well as parts of the microvascular system. **CONCLUSION:** Although cellular details are still beyond the limits of this investigation, the images at 9.4 T show the spinal cord and cervicomedullary junction with detail comparable to low-power microscopic images of fixed sections, especially with respect to distinguishing gray and white matter, nuclei, tracts, and angioarchitecture.

Index terms: Spinal cord, anatomy; Spinal cord, magnetic resonance; Brain stem, anatomy; Brain stem, magnetic resonance

AJNR 14:699–707, May/Jun 1993

In vivo magnetic resonance (MR) imaging of the spinal cord and the brain stem insufficiently reveals the highly complex internal structures. In previous studies, human cadaveric spinal cords were analyzed with 0.35-T to 2-T clinical units (1–7), resulting in images that show limited details compared with corresponding anatomical and histologic sections. In this study, the cervical spinal cord and lower medulla oblongata were imaged with a 9.4-T unit to depict their microanatomical organization in the three spatial dimensions with an in-plane resolution of 40 × 40 microns.

Received December 4, 1991; accepted after revision July 27, 1992.

This work was financially supported by the European Fund for Regional Development and by The Flemish Government.

[1] Department of Anatomy and [2]Institute for Material Research at the Limburg University, B-3590 Diepenbeek, Belgium.

[3] Department of Neurosurgery, University Hospital, Maastricht, The Netherlands.

[4] Department of Radiology, St. Jansziekenhuis, Genk, Belgium.

[5] Address reprint requests to E. A. M. Beuls, MD, Department of Neurosurgery, University Hospital of Maastricht, P. Debeyelaan 25, postbus 5800, 6202 AZ Maastricht, The Netherlands.

AJNR 14:699–707, May/Jun 1993 0195-6108/ 92/1403–0699

Materials and Methods

The cervical spinal cords including the lower medulla oblongata of five adult human cadavers were excised, 12 to 48 hours postmortem. In one case, the entire spinal cord, including the cauda equina, was removed. The specimens were cut into pieces of approximately 3 cm and preserved in saline at 4°C. Imaging experiments were started immediately to keep the preservation period as short as possible. Some spinal cord specimens were preserved in saline for as long as 2 weeks. We chose fresh samples for the examination except for fresh medulla oblongata samples that suffered from a spontaneous collapse during data acquisition and were therefore fixed in 10% formalin.

The MR images were obtained at 4°C with a multisection spin-warp technique on a commercial Varian (Varian, Nuclear Magnetic Resonance Instruments, Palo Alto, CA) Unity 400 spectrometer (9.4 T), equipped with an imaging probe having an inner diameter of 25 mm. For the sagittal and coronal views of the spinal cord and cervicomedullary

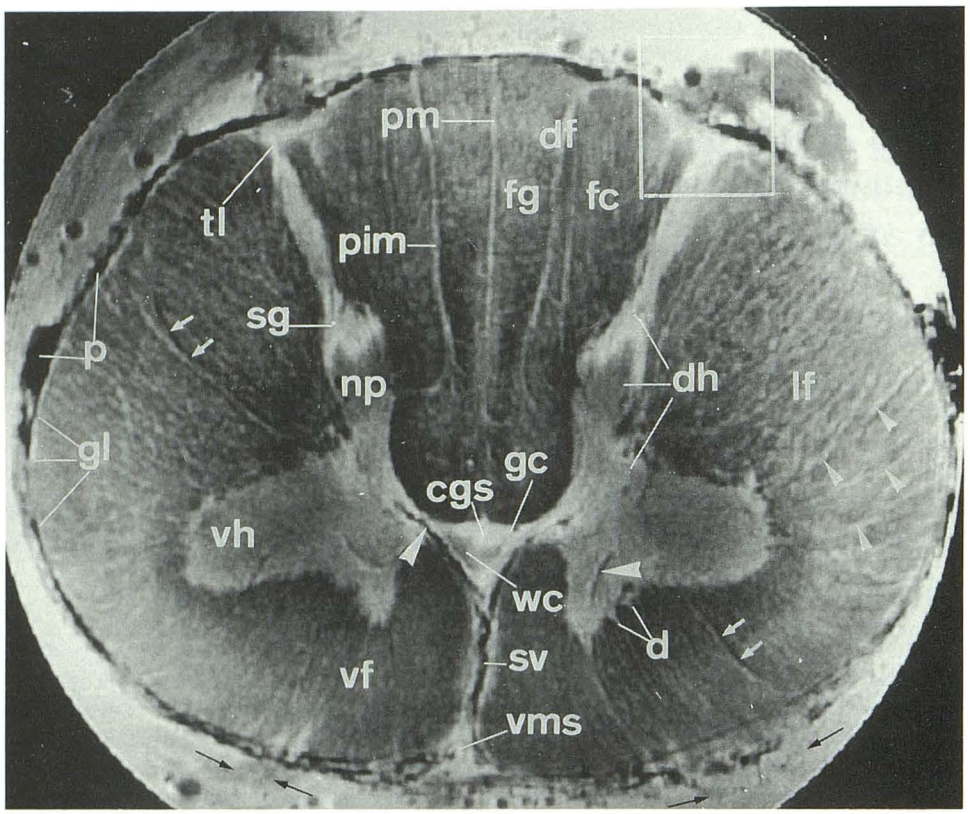

A

Fig. 1*A*. Transverse MR section of the cervical spinal cord at the level of C8. Fresh specimen preserved in saline at 4°C (2500/18/32) (TR/TE/excitations). (*vh*: ventral horn; *gcs*: central gelatinous substance; *gc*: gray commissure; *wc*: white commissure; *dh*: dorsal horn complex; *tl*: tract of Lissauer; *sg*: substantia gelatinosa and marginal layer of Waldeyer; *np*: nucleus proprius; *vf*: ventral funiculus; *lf*: lateral funiculus; fasciculus gracilis (*fg*) and fasciculus cuneatus (*fc*) within the dorsal funiculus (*df*); *vms*: ventral median sulcus; *d*: denticulate aspect of gray matter border; *pm*: posterior median septum; *pim*: posterior intermediate septum; *gl*: glia limitans membrane; *p*: pia mater.) Note the segregation of myelinated and unmyelinated fibers in the dorsal root-spinal cord junction (*square frame*). Ventral rootlets at the surface of the spinal cord (*small black arrows*). Some radially oriented strands of neuroglial framework with high signal intensity are indicated by *small white arrowheads* on the right side of the figure. A large caliber sulcal vessel (*sv*) and branches of sulcal vessels (*large white arrowheads*) in gray matter as well as some small caliber vessels (*small white arrow*) in white matter are seen.

region, 1-mm sections were selected with a field of view of 38 × 17 mm and a data acquisition matrix of 700 × 320. For the transverse images of the spinal cord, 2-mm sections were chosen, while 1-mm sections were taken for those of the cervicomedullary region, all with a field of view of 17 × 17 mm and a data matrix of 350 × 350. This corresponds to an in-plane resolution of 40 × 40 microns. Acquisition parameters of 2500/18 (TR/TE) producing essentially proton density images were used. In one case (see Fig. 2) T2-weighting has been used with a TE of 100 msec. To obtain the required signal-to-noise ratio, 32 excitations were used for the transverse images, and 16 for the sagittal and coronal images, resulting in total acquisition times between 2 and 4 hours. The obtained MR images were compared with myelin-stained sections (Spielmeyer staining technique) (see Fig. 1B) (8) and standard neuroanatomical descriptions (9–12).

Results

The general aspects of the MR appearance of gray and white matter of the spinal cord in transverse sections are first discussed. Next the microanatomy of the more complex dorsal root entry zone, its adjacent dorsal horn complex, and the microvascular system, as well as the appearance of the cervicomedullary region are described.

General MR Appearance of the Spinal Cord in Transverse Sections (Fig. 1A)

The central "gray butterfly" has a higher signal intensity than the surrounding myelinated white

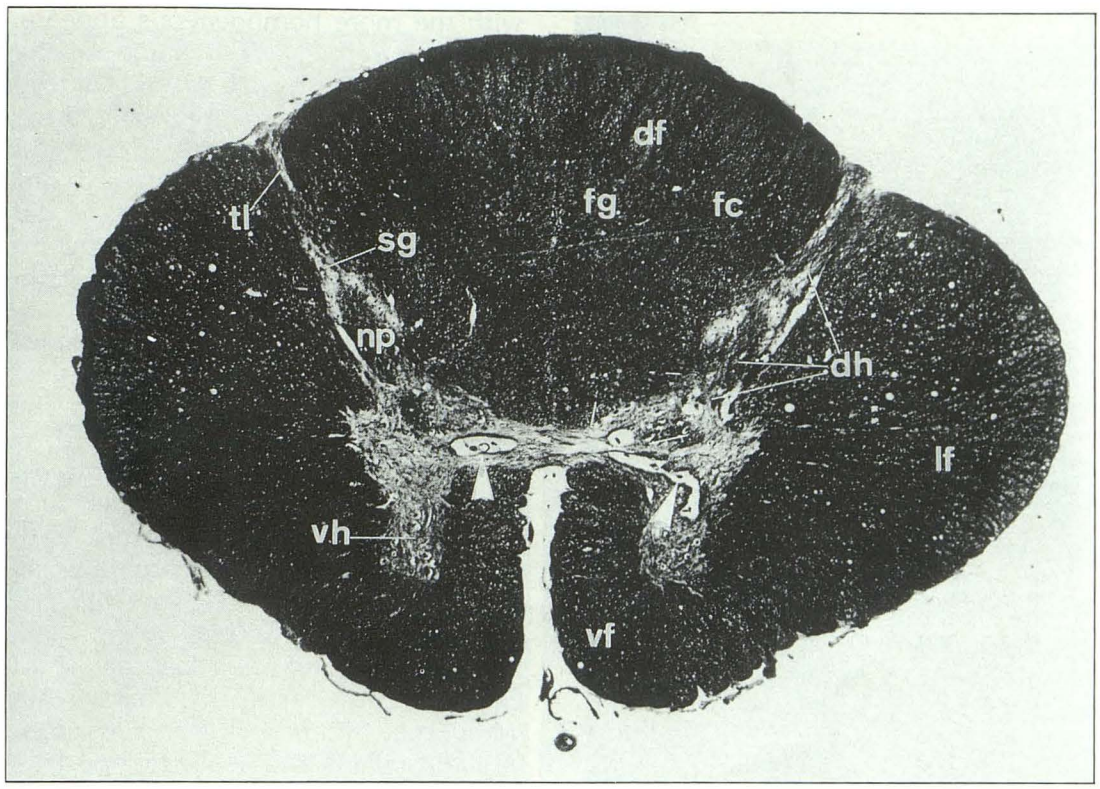

B

Fig. 1.—*Continued. B*, transverse histologic section through the upper cervical segment of the same specimen as in Figure 1A. Spielmeyer stain (10×). (*df*: dorsal funiculus; *fg*: fasciculus gracilis; *fc*: fasciculus cuneatus; *vf*; ventral funiculus; *lf*: lateral funiculus; *dh*: dorsal horn complex; *tl*: tract of Lissauer; *np*: nucleus proprius; *sg*: substantia gelatinosa; *vh*: ventral horn.) Vessels in the gray matter are indicated by *large white arrowheads.*

matter funiculi and can be sharply delineated. This MR aspect is also seen on myelin-stained histologic sections at a higher cervical level (Fig. 1B). There are considerable variations in MR signal intensity in the different parts of the gray butterfly. The ventral horns, composed mainly of cell accumulations in their neuropil, appear as homogeneous, rather intense regions.

The gray commissure is seen as a zone of high signal intensity. Histologically, it contains poorly myelinated and unmyelinated crossing fibers and the central canal, surrounded by the central gelatinous substance or substantia gliosa (9, 10, 13). The white commissure, which is the decussating site of large extralemniscal myelinated fibers, is seen as a zone of low signal intensity.

The tract of Lissauer or fasciculus dorsolateralis, which lies between the apex of the dorsal horn and the surface of the spinal cord and which is composed of poorly myelinated and unmyelinated fibers, has a much higher signal intensity than the surrounding myelinated white matter. Only in some sections can it be distinguished from the adjacent dorsal horn. A somewhat dark regular ring segment, which is surrounding the central structures, does not correspond to any known anatomical feature. This ring is an acquisition artifact caused by analog-to-digital convertor overflow (the receiver gain was set somewhat too high in the first experiments).

In the ventral and lateral funiculus, no individual tracts can be distinguished. In the dorsal funiculus, the fasciculus gracilis shows a slightly higher signal intensity compared with the fasciculus cuneatus. This higher signal intensity has been reported in previous investigations (6). In transverse sections, strands of high signal intensity are radially extended between the glia limitans membrane and the border of the gray butterfly (Fig. 1A). The glia limitans is a layer of neuroglia beneath the pia mater, showing high signal intensity. The pia appears black. The connection between these neuroglial strands of high signal intensity and the border of the gray matter

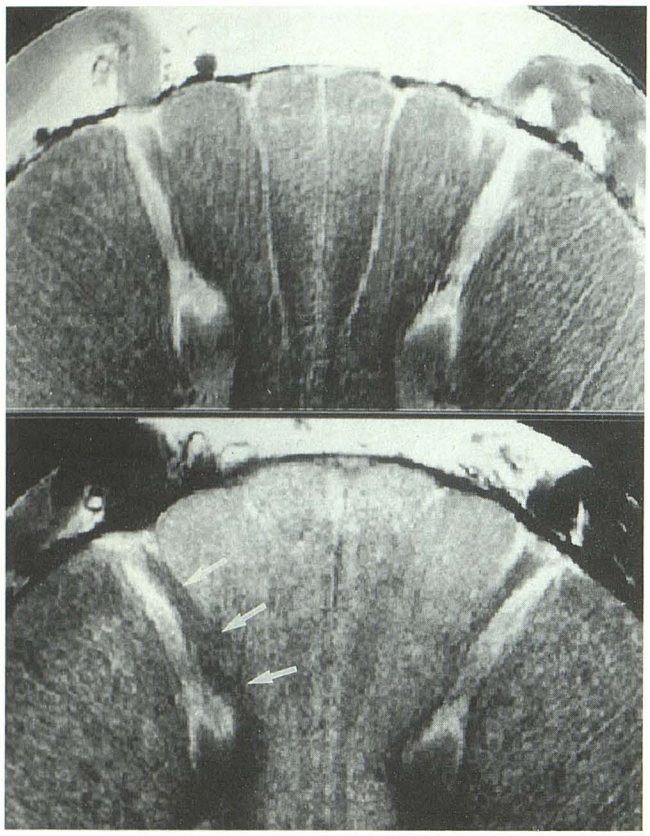

Fig. 2. Transverse MR sections though the dorsal root entry zone of the fresh cervical spinal cord to illustrate the difference between proton density (top: 2500/18/32) and T2-weighted (bottom: 2500/100/32) images. Note the course of the segregated myelinated entering bundles, demonstrated on the T2-weighted images (*arrows*), while the neuroglial framework is most appearant on the proton density images.

offers the latter a denticulate aspect. The strands cannot be traced inside the gray matter columns. Inside the white matter, they are irregularly interconnected, forming a neuroglial framework. This framework is, apart from the posterior median and intermediate septum, hardly mentioned in standard anatomical descriptions of the spinal cord white matter (9, 10). Histologically, these neuroglial elements are formed by radial processes of fibrous astrocytes, running in fascicles throughout the white columns (9, 10, 13).

Finally, ventral rootlets, passing through the ventral funiculus, can hardly be seen. Their penetration through the pial surface is somewhat more visible.

The Dorsal Horn Complex

The MR images of the dorsal horn and its adjacent dorsal-root entry zone contrast strongly with the more homogeneous appearance of the ventral horn (Fig. 1A). It is not possible to distinguish the marginal layer of Waldeyer and the substantia gelatinosa because they have an equally high signal intensity. The tract of Lissauer or dorsolateral fascicle, having a slightly lower signal intensity, cannot always be differentiated from the substantia gelatinosa. The nucleus proprius is easy to define because of its lower signal intensity.

As the central processes of the spinal ganglion cells approach the dorsal-root entry zone they become segregated according to their caliber. Large-caliber, myelinated fibers form a medial bundle; small-caliber fibers, unmyelinated and poorly myelinated, shift mainly to the lateral portions of the rootlets. Some of these small caliber fibers, however, occupy a position medial to the entering rootlets. The large fibers pass between the posterior gray column and the dorsal white column and there they divide into ascending branches, joining the dorsal white column, and descending branches forming the fasciculus interfascicularis and septomarginalis. The small-caliber fibers join the tract of Lissauer (14–16). In the proton density transverse sections (Fig. 2, top) no clear distinction can be made between the medial bundle of large myelinated fibers, passing along the medial side of the posterior horn, and the dorsal white column. The small medial bundle of segregated small fibers represents the separation between both. By the application of some T2 weighting (TE = 100 msec), the medial bundle is seen better (Fig. 2, bottom).

In the sagittal section through the dorsal-root entry zone (Fig. 3A) well-demarcated entering bundles of low signal intensity are seen to run 2 to 3 mm upwards. Before these bundles disappear in the cuneate fascicle, the continuation of their ascending course is observed, medial to the dorsal horn, over about 0.5 mm in the corresponding coronal section though the apex of the posterior horn (Fig. 3B).

Internal Vascularization

The MR images also depict parts of the internal vascularization of the spinal cord. In the absence of flow, paramagnetic T2 shortening caused by iron ions in the erythrocytes and blood clot formation may account for the appearance of the angioarchitecture.

While large-caliber vessels are located in the ventral median sulcus, with their branches di-

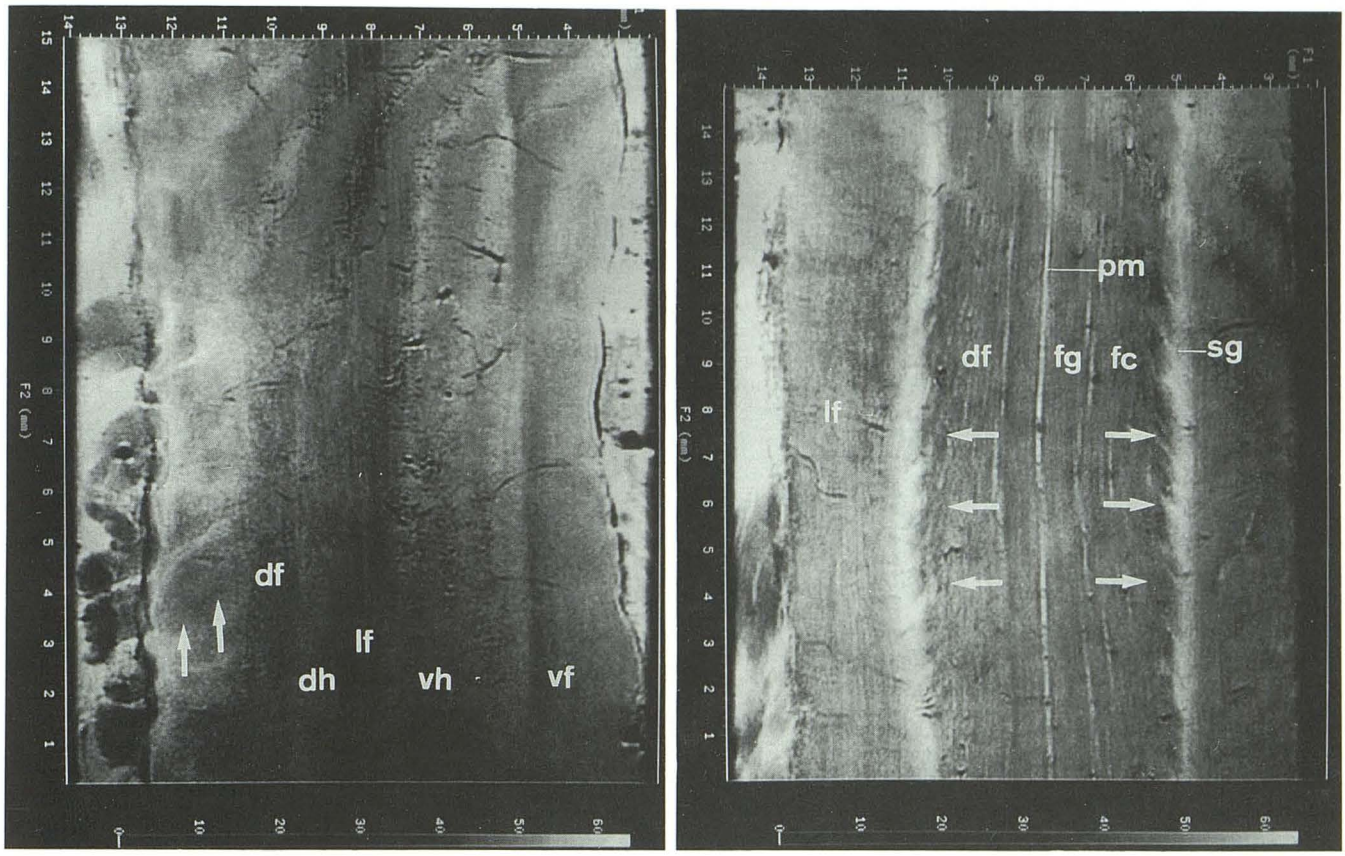

Fig. 3. Longitudinal MR sections at the top of the dorsal horn of the lower cervical medulla spinalis (C6-C8) illustrate the dorsal-root entry zone. Fresh specimen preserved in saline 4°C. (2500/18/16). *White arrows* indicate the slightly ascending course of the segregated myelinated fibers before they join the dorsal funiculus (*df*).

A, Sagittal section. (*dh*: dorsal horn; *lf*: lateral funiculus; *vh*: ventral horn; *vf*: ventral funiculus.)

B, Coronal section. (*lf*: lateral funiculus; *fg*: fasciculus gracilis; *fc*: fasciculus cuneatus; *sg*: substantia gelatinosa; *pm*: posterior median septum.)

rected towards the ventral horns (Fig. 1A), small-caliber vessels are present throughout the white matter. The latter are radially oriented between the surface of the spinal cord and the border of the gray butterfly, often following the strands of neuroglial framework. The difference in the caliber of the vessels is best appreciated in the sagittal section (Fig. 4A). In the coronal section just ventral to the central canal (Fig. 4B), branches of the sulcal vessels pass nearly alternately to the left and to the right.

The Cervicomedullary Region

Most of the commonly known microstructures seen in standard histologic sections (9–12) are sharply delineated and can be identified in consecutive 1-mm sections (Figs. 5A and 5B) in the cervicomedullary region.

The coronal and sagittal images (Figs. 5C and 5D) show the gray columns, the reticular formation, the major nuclei of the medulla oblongata, and the principal white matter tracts. Two of the most conspicious features of the cervicomedullary transition, the decussation of the corticospinal fibers and of the lemnisci, are particularly well demonstrated in both coronal and sagittal sections (Figs. 5C and 5D).

The corticospinal fibers cross the midline in interdigitating bundles, running in a steep dorsocaudal direction across the anterior gray column. The decussation extends over a length of 12 to 13 mm. The most caudal pyramidal fibers cross in the upper cervical spinal segment. The lateral corticospinal tract shows an abundance of hyper-

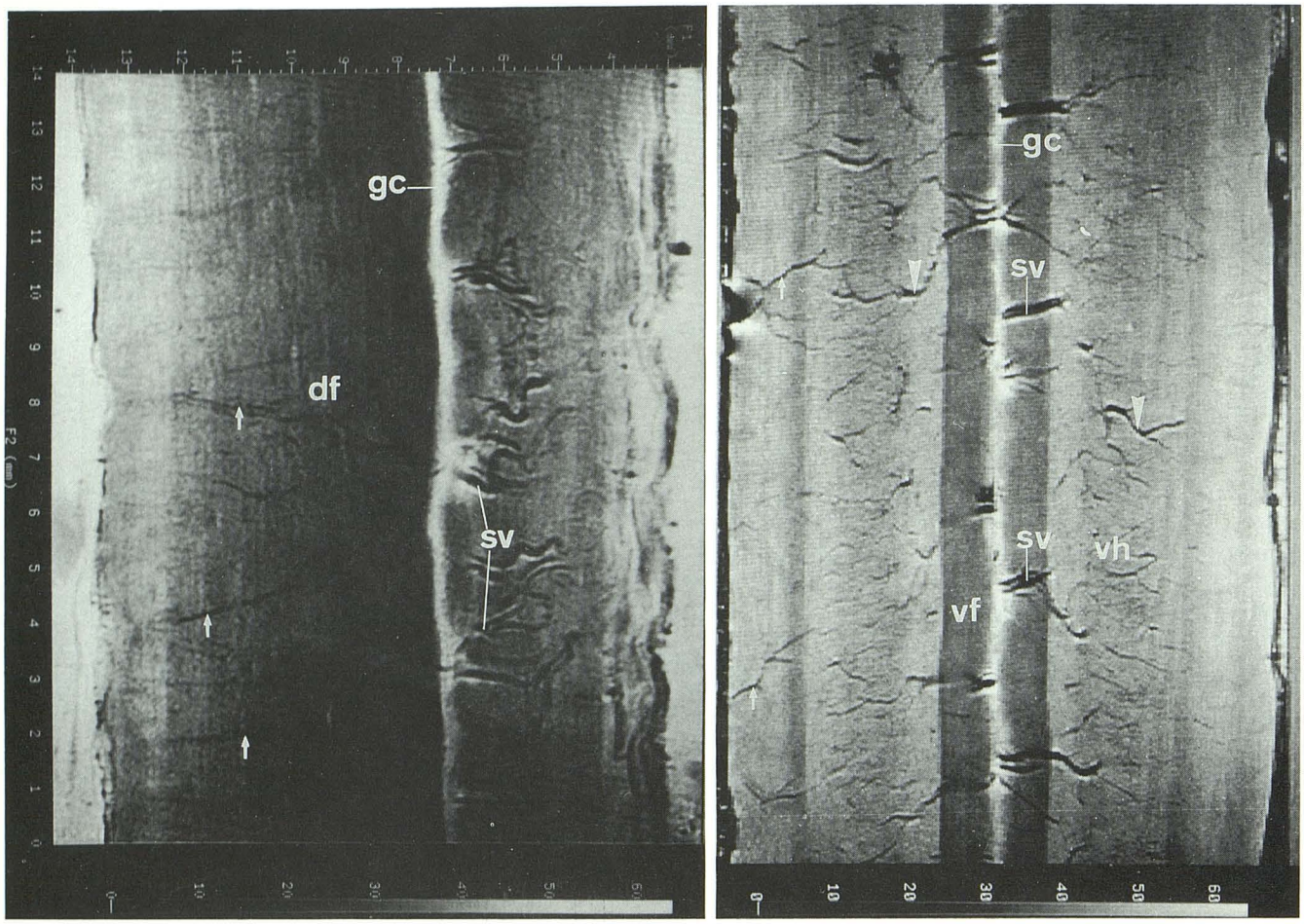

Fig. 4. Longitudinal MR sections of the lower cervical medulla spinalis (C6-C8) showing the internal vascularization of gray and white matter (2500/18/16). Fresh specimen preserved in saline at 4°C (2500/18/16). No distinction can be made between arteries and veins.

A, Midsagittal section also showing the large caliber sulcal vessels (*sv*) and small caliber vessels (*small arrows*) in the white matter of the dorsal funiculus (*df*). (*gc*: gray commissure.)

B, Coronal section through the ventral horn (*vh*) shows large-caliber sulcal vessels (*sv*) and parts of their arborizations (*arrowheads*) in the ventral horns as well as small caliber vessels (*small arrows*) in white matter. Note that branches of sulcal vessels pass almost alternately to the left and to the right. (*gc*: gray commissure; *vf*: ventral funiculus; *lf*: lateral funiculus.)

intense longitudinal strands of neuroglial framework.

The fascicles of the dorsal white columns progressively decrease in size as their nuclei become more prominent. The gracile nucleus occupies a more medial position (Fig. 5B) than the cuneate nucleus. Myelinated internal arcuate fibers, leaving the ventral parts of these nuclei, can be followed towards the lemniscal decussation. Although these fibers are usually described as sweeping ventromedially around the central gray (9, 10), they actually are seen to run ventrorostrally in parallel with the decussated corticospinal fibers (Fig. 5D).

Discussion

The high definition of the MR images in this postmortem investigation exceeds that of clinical imaging for a number of reasons. The lack of motion, the relatively small radio frequency coil, the stable linearity of the gradient fields, and the high main magnetic field (9.4 T) lead to an increased signal-to-noise ratio. The ability to use long acquisition times (16 or more repetitions) also contributes to the optimal image appearance.

To avoid shrinkage and deformation of specimens, we investigated the human spinal cord using the freshest specimens possible. The fresh

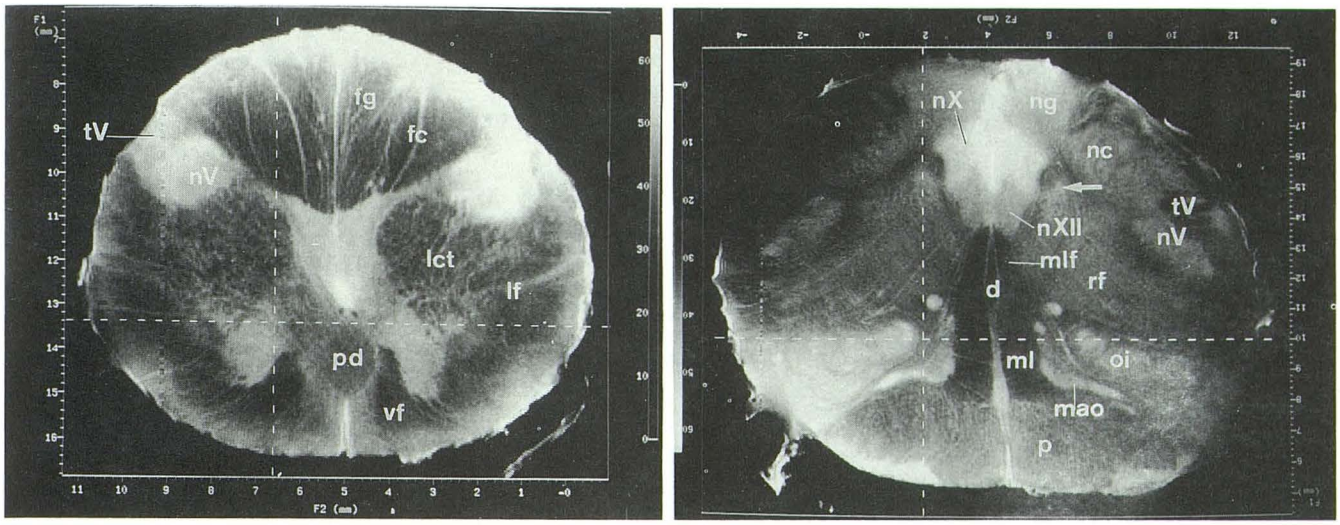

Fig. 5. MR sections through the cervicomedullary junction of a 10% formalin-fixed specimen.

A, Transverse MR section (2500/18/32) through the cervicomedullary transition at the level of the pyramidal decussation (*pd*). Note the characteristic appearance of the white funiculi caused by their different pattern of neuroglial framework. (*lct*: lateral corticospinal tract; *fg*: fasciculus gracilis; *fc*: fasciculus cuneatus; *vf*: ventral funiculus; *lf*: lateral funiculus; *nV*: nucleus of the spinal tract of the trigeminal nerve; *tV*: spinal tract of the trigeminal nerve.)

B, Transverse MR section (2500/18/32) through the medulla oblongata at the level of the olivary complex allowing the identification of inferior olivary nucleus (*oi*); (*mao*: medial accessory olivary nucleus; *nXII*: hypoglossal nucleus; *nX*: dorsal nucleus of vagal nerve; *ng*: nucleus gracilis; *nc*: nucleus cuneatus; *nV*: spinal nucleus of trigeminal nerve; *rf*: reticular formation; *ml*: medial lemniscus; *d*: lemniscal decussation; *p*: pyramidal tract; *tV*: spinal tract of trigeminal nerve; *mlf*: medial longitudinal fascicle and the nucleus of the tractus solitarius (*arrow*).)

medulla oblongata, however, suffered from a spontaneous collapse during the data acquisition process. This slow movement prevented us from obtaining the desired image definition. For this reason, we decided to fix the medulla oblongata specimens to properly immobilize them. Previous studies on fresh and fixed brain stems, using a clinical instrument, report an improved gray-white differentiation after fixation (2, 4).

Proton density images show low intensity for the heavily myelinated ventral, lateral, and dorsal funiculus. This is in accordance with the results of previous in vivo (17) and in vitro studies (1, 3, 6, 7, 18). This is consistent with partial displacement of signal-producing water protons by myelin (19). The longitudinal arrangement of the myelinated fiber might be another element in the low signal intensity of the white matter (1).

The neuroglial framework, which is clearly visualized using proton density sequences, cannot be demonstrated in T2-weighted images (Fig. 2). The dependence on the echo time reflects its highly structured organization. This neuroglial framework has received little attention in the anatomical descriptions of the spinal cord, most likely because it has not been visualized by most staining techniques. Despite the attention Cajal (20) drew to the neuroglia, only a few authors made anatomical descriptions of the extension of the neuroglia in the nervous tissue of the spinal cord. Bossy (21) gave a rather complete anatomical description. In the proton density MR images, the neuroglial framework appears similar to these histologic descriptions in the literature. The presence of this dense neuroglial framework might explain the difference in signal intensity between the spinal and cerebral white matter in clinical imaging (2, 17). In the longitudinal sections, made at the level of the substantia gelatinosa (Fig. 3B), the course of the medially segregated myelinated bundle of the dorsal root is seen ascending over 2 to 3 mm. This course has not been reported in anatomic descriptions of the dorsal-root entry zone (14–16).

The MR images also reproduce an angioarchitecture corresponding to vessel arrangements in the spinal cord (22). The dark MR appearance of vessels in the postmortem specimens is probably due to the presence of paramagnetic iron ions in the erythrocytes and the formation of blood clots.

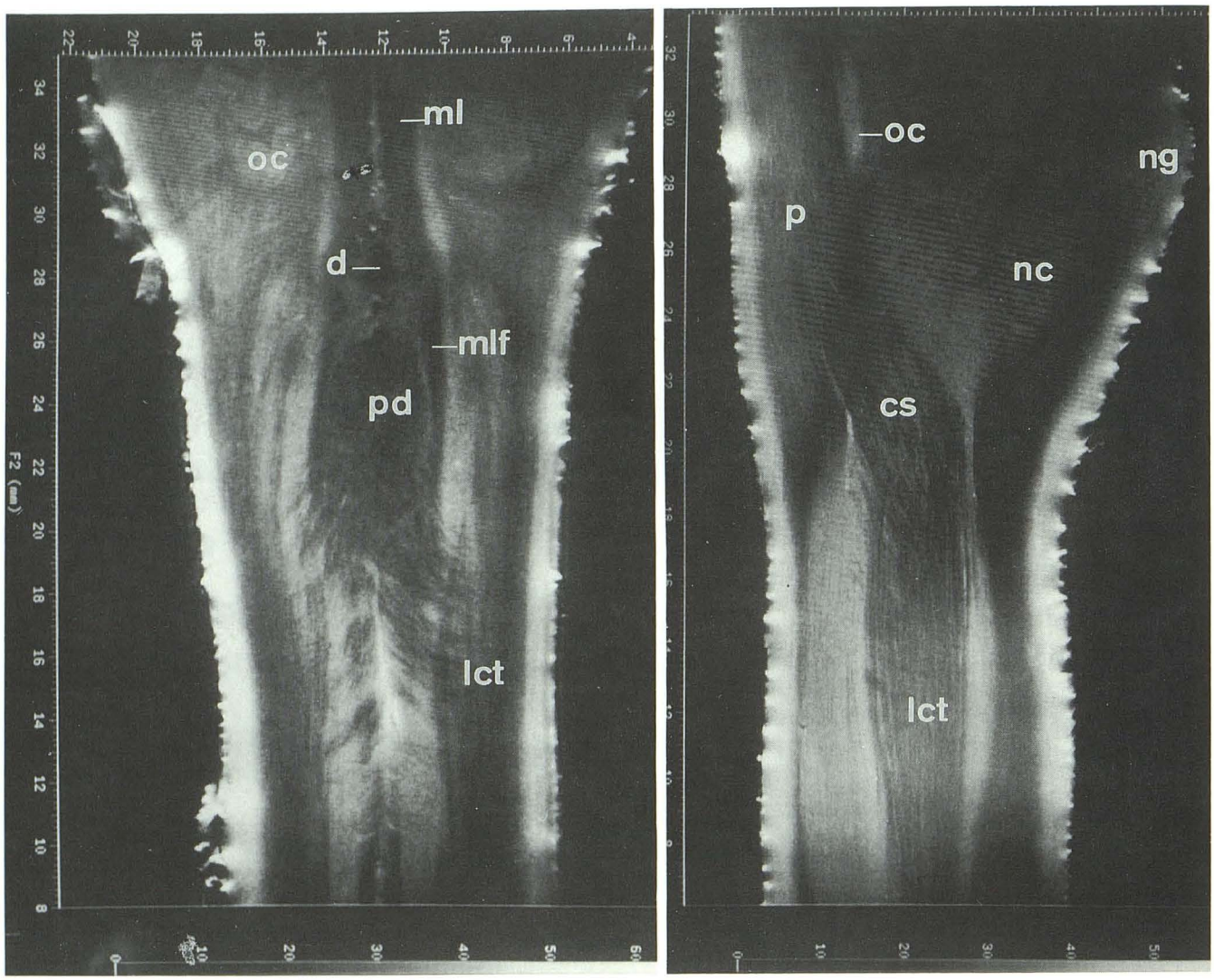

Fig. 5.—*Continued. Coronal (C)* and sagittal (*D*) MR sections (2500/18/16) through the cervicomedullary transition. The location of these sections is indicated in Figures 5A and 5B.

C, Shows the crossing and descending fibers from the pyramidal decussation (*pd*) to the lateral corticospinal tract (*lct*). Immediately above the pyramidal decussation, the lemniscal decusation (*d*) and the medial longitudinal fascicle (*mlf*) are visible. More rostrally the olivary complex (*oc*) and the medial lemniscus (*ml*) are seen.

D, Internal arcuate fibers leave the nucleus gracilis (*ng*) and nucleus cuneatus (*nc*) and run anterosuperiorly and parallel to the crossed, descending corticospinal fibers (*cs*). The latter reach the lateral corticospinal tract (*lct*). In the rostral part the pyramidal tract (*p*) and the olivary complex (*oc*) are depicted. Note the hyperintense strands of neuroglial framework in the lateral corticospinal tract.

Acknowledgments

We wish to thank Professor J. J. Martin (University of Antwerp) for the preparation of the histologic sections. We also thank J. Thys and M. Theunissen for typing the manuscript.

References

1. Curtin AJ, Chakeres DW, Bulas R, Boesel CP, Finneran M, Flint E. MR imaging artifacts of the axial internal anatomy of the cervical spinal cord. *AJNR: Am J Neuroradiol* 1989;152:835–842
2. Carvlin MJ, Asato R, Hackney DB, Kassab E, Joseph PM. High-resolution MR of the spinal cord in humans and rats. *AJNR: Am J Neuroradiol* 1989;10:13–17
3. Flannigan BD, Bradley WG, Mazziotta JC, et al. Magnetic resonance imaging of the brainstem: normal structure and basic functional anatomy. *Radiology* 1985;154:375–383
4. Hirsch WL, Kemp SS, Martinez AJ, Curtin H, Latchaw RE, Wolf G. Anatomy of the brainstem: correlation of in vitro MR images with histologic sections. *AJNR: Am J Neuroradiol* 1989;10:923–928
5. Ho PSP, Yu S, Czervionke LF, et al. MR appearance of gray and white matter at the cervicomedullary region. *AJNR: Am J Neuroradiol* 1989;10:1051–1055

6. Solsberg MD, Lemaire C, Resch L, Potts DG. High-resolution MR imaging of the cadaveric human spinal cord: normal anatomy. *AJNR: Am J Neuroradiol* 1990;11:3–7
7. Solsberg MD, Fournier D, Potts DG. MR imaging of the excised human brainstem: a correlative neuroanatomic study. *AJNR: Am J Neuroradiol* 1990;11:1003–1013
8. Heym CH, Forsmann WG. *Techniques in neuroanatomical research.* New York: Springer-Verlag, 1981:14–15
9. Carpenter MB, Suttin J. *Human neuroanatomy.* 8th ed. Baltimore: Williams & Wilkins, 1983;233:357, 707–712
10. *Gray's anatomy.* 37th ed. New York: Churchill Livingstone, 1989:919–961
11. Nieuwenhuys R, Voogd J, Van Huyzen C. *The human central nervous system.* 3rd ed. Berlin: Springer-Verlag, 1988:132–139
12. Miller RA, Burack E. *Atlas of the central nervous system in man.* 2nd ed. Baltimore: Williams & Wilkins, 1977
13. Ham AW. *Histology.* 7th ed. Phildelphia: J.B. Lippincott, 1974:496
14. Sindou M, Quoex C, Baleydier C. Fiber organization at the posterior spinal cord-rootlet junction in man. *J Comp Neurol* 1974;153:15–26
15. Sindou M, Goutelle A. Surgical posterior rhizotomies for the treatment of pain. *Adv Tech Stand Neurosurg* 1983;10:147–185
16. Gybels JM, Sweet WH. Neurosurgical treatment of persistent pain. *Pain Headache* 1989;11:125–150
17. Czervionke LF, Daniels DL. Cervical spine anatomy and pathologic processes: applications of new MR imaging techniques. *Radiol Clin North Am* 1988;26,5:921–947
18. Lemaire C, Duncan EG, Solsberg MD, Armstrong RL. In vitro magnetic resonance microimaging of the spinal cord. *Magn Res Med* 1990;14:97–104
19. Enzmann DR, DeLaPaz RL, Rubin JB. *Magnetic resonance of the spine.* St. Louis: C. V. Mosby, 1990:108–126
20. Cajal RS. *Histologie du système nerveux de l'homme et des vertèbres.* Edition française revue et mise à jour par l'auteur. Madrid: C.S.I.C., Instituto Ramon Y Cajal. 1952;1:230–252
21. Bossy J. *Anatomie clinique: neuro-anatomie.* Paris: Springer-Verlag, 1990:319–324
22. Lazorthes G, Gouaze A, Djindjian R. *Vascularisation et circulation de la moelle épinière.* Paris: Masson, 1974:41–125